ADVANCED MATERIALS TECHNOLOGIES
www.advmattechnol.de

Elastomeric Optical Waveguides by Extrusion Printing

*Jun Feng, Yijun Zheng, Qiyang Jiang, Małgorzata K. Włodarczyk-Biegun, Samuel Pearson, and Aránzazu del Campo**

Advances in optogenetics and the increasing use of implantable devices for therapies and health monitoring are driving demand for compliant, biocompatible optical waveguides and scalable methods for their manufacture. Molding, thermal drawing, and dip-coating are the most prevalent approaches in recent literature. Here the authors demonstrate that extrusion printing at room temperature can be used for continuous fabrication of compliant optical waveguides with polydimethylsiloxane (PDMS) core and crosslinked Pluronic F127-diacrylate (Pluronic-DA) cladding. The optical fibers are printed from fluid precursor inks and stabilized by physical interactions and photoinitiated crosslinking in the Pluronic-DA. The printed fibers show optical loss values of 0.13–0.34 dB cm^{-1} in air and tissue within the wavelength range of 405–520 nm. The fibers have a Young's Modulus (Pluronic cladding) of 150 kPa and can be stretched to more than 5 times their length. The optical loss of the fibers shows little variation with extension. This work demonstrates how printing can simplify the fabrication of compliant and stretchable devices from materials approved for clinical use. These can be of interest for optogenetic or photopharmacology applications in extensible tissues, like muscles or heart.

1. Introduction

Optical waveguides can be used for delivering light from an external light source to within the human body for therapies like photodynamic therapy or optogenetics.[1] In advanced waveguides, light delivery can be coupled with biosensing functions, in which optical/electrical signals are transported in the opposite direction by the same waveguide and used for diagnostics. In most cases, such waveguides are fabricated in batch processes with sequential layer depositions and precise curing/etching steps adapted from silicon-based microelectronics.[2] From a manufacturing perspective, continuous, higher-throughput production methods are needed to move towards integration of additional capabilities in a single production process. Impressive progress has been demonstrated on the fabrication front by Anikeeva and co-workers, who have produced multifunctional optical fibers[3] that incorporate optical waveguides, microfluidic channels, and electrodes by thermal drawing of thermoplastics.[4] From a patient comfort perspective, biomedical waveguides also need to move away from silica and thermoplastics to more compliant materials in order to improve in vivo biocompatibility by matching the stiffness of the target tissue.[1,5] To be applied to optogenetic activation in tissues like muscles or heart, the optical fibers need to have an elastomeric character and be extensible. Silicone elastomers such as polydimethylsiloxane (PDMS) are interesting candidates, offering stiffness values in the low MPa range[6] and proven track records as biocompatible implant materials.[7] The optical properties of PDMS are well suited to waveguiding: PDMS has a low optical loss coefficient from UV to NIR wavelengths (≤0.05 dB cm^{-1} at 850 nm)[8] and a relatively high refractive index (RI ≥ 1.40).[8,9] In addition, PDMS shows high extensibility (>100%) and tensile strength (>1 MPa),[10] offering compliance and stretchability for high movement scenarios in the body.[4c,11] The importance of light delivery and retrieval under high strain has been demonstrated using stretchable optical devices for a range of biomedical scenarios such as strain sensing in prosthetics[12] and optogenetic stimulation of peripheral nerves[11b] and spinal cord.[4c]

PDMS-based waveguides have been explored in devices employed at the periphery of the body. Ribbon-shaped PDMS waveguides produced by mold-casting have been developed to photocrosslink the sclera of the eye to stave off myopia,[13] with the compliance and stretchability of PDMS allowing correct

J. Feng,[+] Y. Zheng,[++] Q. Jiang,[+++] M. K. Włodarczyk-Biegun,[++++] S. Pearson, A. del Campo
INM – Leibniz Institute for New Materials
Campus D2 2, 66123 Saarbrücken, Germany
E-mail: aranzazu.delcampo@leibniz-inm.de
J. Feng, Q. Jiang, A. del Campo
Chemistry Department
Saarland University
66123 Saarbrücken, Germany
M. K. Włodarczyk-Biegun
Biotechnology Centre
The Silesian University of Technology
Bolesława Krzywoustego 8, Gliwice 44-100, Poland
The ORCID identification number(s) for the author(s) of this article can be found under https://doi.org/10.1002/admt.202101539.

[+]Present address: Institut für Chemie und Biochemie – Organische Chemie, Freie Universität Berlin, Takustrasse 3, 14195 Berlin, Germany
[++]Present address: School of Physical Science and Technology, ShanghaiTech University, Shanghai 201210, China
[+++]Present address: Institute for Molecular Systems Engineering (IMSE), Heidelberg University, 69120 Heidelberg, Germany
[++++]Present address: Polymer Science, University of Groningen, Nijenborgh 4, Groningen 9747AG, The Netherlands

DOI: 10.1002/admt.202101539

waveguide positioning under the ocular muscles without causing mechanical damage. A 1 mm thick ribbon waveguide exhibited a loss coefficient of 0.5 dB cm^{-1} at 445 nm when in contact with scleral tissue. Dye-doped PDMS optical fibers fabricated by molding have been used to sense and quantify large joint movements and subtle movements like breathing and speech by exploiting the linear increase in optical loss (in dB) of the PDMS waveguide with elongation.[14] PDMS-based thin-film waveguides fabricated by molding have been demonstrated as pressure-sensitive artificial skin that could detect a light finger touch (≈1 kPa).[15] Other PDMS-based strain[9b,14,16] and pressure[9a,15] sensors have quantified movement in a similar manner by measuring light loss upon stretching or compression.[12,16] Core/cladding PDMS fibers produced by molding and dip-coating have been used to sense skin temperature during physical exertion courtesy of upconversion nanoparticles (UCNPs) embedded in the core.[6] This waveguide showed an optical loss of 1.2 dB cm^{-1} at 500 nm, and the PDMS formulations used for the core and the cladding had RIs of 1.424 and 1.417, respectively.[6] The PDMS core/cladding design seems appropriate for applications inside the body since the cladding would reduce disturbance from surrounding tissue. Developing a more straightforward fabrication of PDMS-based core/cladding waveguides that also exhibit a greater RI difference between core and cladding and lower optical loss are key challenges to improving PDMS-based waveguides for in vivo applications that motivated the present work.

The most widely-used PDMS precursors crosslink via hydrosilylation reactions between H-bearing and vinyl-bearing polysiloxane chains and offer the advantage of being optically transparent over a large wavelength range well into the UV region. However, the reaction is too slow to be efficiently used in a continuous fiber fabrication process.[6,17] PDMS fibers have been produced by fiber drawing[18] but this required partial precuring of the precursor mixture, which is difficult to control and therefore inappropriate for a continuous manufacturing process. Commercially-available acrylated polysiloxane prepolymers are an alternative that could facilitate in situ photocrosslinking in an extrusion process,[19] but these precursors show lower transparency at UV wavelengths. In this paper, we describe an extrusion-based printing process that allows continuous fabrication of core/cladding waveguides from PDMS precursors that cure by hydrosilylation using extrusion printing. The process uses acrylated Pluronic F-127 as cladding material for the optical function and as template material to aid PDMS printing.

Pluronics are clinically-approved ABA triblock copolymers consisting of poly(ethylene oxide) (PEO) and poly(propylene oxide) (PPO) that can self-assemble into micelles at concentrations >2.8 μM at 37 °C in water.[20] One of the key features of Pluronic solutions is their thermoreversible behavior at higher concentrations.[21] Pluronic F-127 solutions at concentrations above ≈20 wt.% undergo a sol-gel transition at around room temperature due to dehydration of the hydrophilic PEO shell blocks at higher temperatures, resulting in close-packing of Pluronic micelles to form compliant physical gels.[22] Pluronic gels exhibit shear thinning, which is beneficial for extrusion,[23] and retain their printed shape when shear forces cease. Pluronic can be used as a sacrificial material for co-extrusion of slow-polymerizing inks,[24] after which the Pluronic layer can be removed from the cured core by simply decreasing the temperature. Alternatively, acrylate end-functionalized Pluronic F127 (Pluronic-DA) can be used, since it offers similar rheological properties to unmodified Pluronic while permitting in situ photopolymerization during printing to form a cladding layer.[25] While crosslinked networks containing low concentrations (<10 wt.%) of Pluronic-DA are not completely transparent due to network inhomogeneities,[26] Pluronic-DA gels (>20 wt.%) show high transparency that is maintained after photocrosslinking.[27] Crosslinked Pluronic-DA exhibits lower RI than PDMS (RI < 1.4 for Pluronic gels at < 50 wt.%)[28] and elastomeric mechanical properties.[26a,29] Pluronic-DA, therefore, appears to be a suitable cladding material in elastomeric PDMS-based core/cladding waveguides for in vivo applications. In previous research, Pluronic-DA has been successfully employed as cladding layer to print PEG-based optical fibers.[25] In this work, we demonstrate the capability to use Pluronic-DA as a cladding layer to print elastomeric optical fibers.

2. Results and Discussion

2.1. Synthesis and Physicochemical Properties of Pluronic-DA and PDMS

Pluronic-DA was synthesized following a reported method[30] by reacting the terminal hydroxyl groups of Pluronic F-127 with acryloyl chloride (Scheme S1, Figures S1A and S1B, Supporting Information), giving a degree of substitution of 70%. The transition temperatures of Pluronic-DA solutions in water at 16.7–33.3 wt.% were determined by rheology. The characteristic sigmoidal evolution of G' and G'' over the temperature range of 5 to 37 °C (Figure S2A, Supporting Information) confirmed the sol-gel transition,[22b] with the transition temperature decreasing with increasing polymer concentration (Table S1, Supporting Information). At the concentrations of 23.1 wt.% and greater, the transition temperatures were below room temperature, which is an interesting range for printing Pluronic-DA under ambient conditions. As a physical gel, Pluronic-DA also shows decreasing viscosity with increasing shear rate (Figure S2B, Supporting Information), revealing shear-thinning behavior known to facilitate extrusion and the maintenance of structure post-extrusion.[23]

The mechanical properties of 23.1–33.3 wt.% Pluronic-DA hydrogels before and after photoinitiated crosslinking of the DA groups were analyzed by rheology (Table S1 and Figure S2C, Supporting Information). The Young's modulus ranged from 71–151 kPa after photopolymerization, while swelling ratios decreased with increasing polymer contents—from 1082% at 23.1 wt.% to 759% at 33.3 wt.% (Table S1, Supporting Information)—as expected from higher crosslinking degrees.[31]

Thermal- and UV-curable PDMS (Sylgard 184 from Dow Corning, denoted T-PDMS, and KER 4690 from Shin-Etsu, denoted UV-PDMS, respectively) were used in this work. At room temperature, both PDMS precursors are viscous liquids (viscosity 3.5 Pa.s for T-PDMS and 2.7 Pa.s for UV-PDMS; data from manufacturers). Both PDMS precursors form elastomeric networks via Pt-catalyzed hydrosilylation between Si-H- and

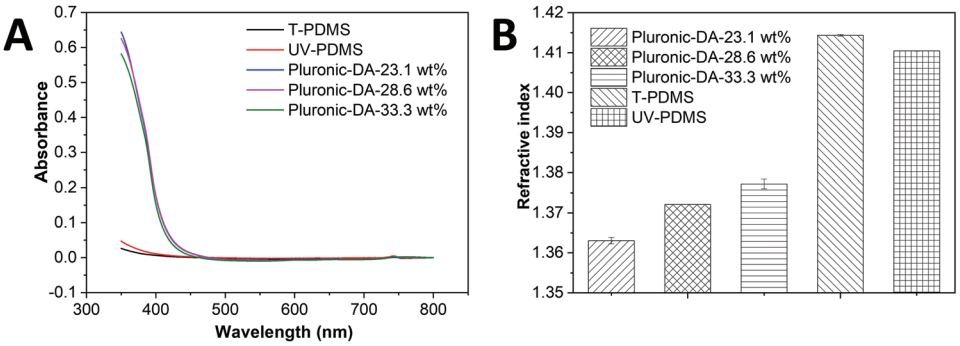

Figure 1. A) Absorbance spectra of cured PDMS and covalently-crosslinked Pluronic-DA hydrogels at different concentrations. B) Refractive index (RI) of cured PDMS and covalently-crosslinked Pluronic-DA hydrogels at different concentrations. Data are presented as average ± standard deviation ($n = 3$).

Si-vinyl-bearing polysiloxane pre-polymers.[32] According to the manufacturers, T-PDMS requires 48 h to cure at room temperature[33] while UV-PDMS requires 2000 mJ cm^{-2} of UV exposure for activation followed by 24 h at room temperature for full curing. The formed elastomers were expected to demonstrate high flexibility and stretchability (elongation at break > 100%), and tensile strengths in the MPa range.

2.2. Optical Properties of PDMS and Pluronic-DA Bulk Materials

To characterize the optical properties of the T-PDMS and UV-PDMS elastomers and the Pluronic-DA hydrogels, samples were prepared in standard 1 cm wide poly(methyl methacrylate) disposable cuvettes. The transparency of the materials was evaluated by UV–vis spectroscopy, giving the intrinsic light loss from scattering and absorption combined. Both cured PDMS materials showed high transparency in the wavelength range from 350 nm to 800 nm (**Figures 1**A; Figure S3A, Supporting Information), which is essential for their use as waveguiding materials. UV-PDMS showed slightly higher absorbance than T-PDMS at wavelengths <400 nm, presumably due to absorption by species associated with the photoactivatable catalyst. Pluronic-DA hydrogels were transparent at wavelengths >450 nm but showed strong absorbance below 450 nm (Figure 1A). This is attributed to scattering from the nano-scale micellar structures. Slight scattering effects were also observed in PDMS in independent scattering measurements at 520 nm (Figure S3B, Supporting Information). These are attributed to fluctuations/inhomogeneities in the network composition and are not significant for the optical performance of the system. Overall, these results show that the selected PDMS materials exhibit low intrinsic optical losses suitable for waveguide cores and that Pluronic-DA hydrogels intended as cladding materials are also highly transparent in the visible range.

The difference between the RIs of the core and cladding materials is a key factor determining the optical confinement in waveguides. Light confinement in the core via total internal reflection requires it to have a higher RI than that of the cladding. The RIs of Pluronic-DA hydrogels were measured to be 1.363 and 1.377 at concentrations of 23.1–33.3 wt.%. These values are lower than those of T-PDMS (1.414) and UV-PDMS (1.410) (Figure 1B). The RI difference between the two materials is appropriate for fabricating step-index optical waveguides with Pluronic-DA at any of the tested concentrations as cladding and either of the PDMS types as core.

2.3. Printing Core/Cladding Optical Waveguides

A commercial printer equipped with an extrusion head bearing a coaxial needle (inner needle: 22G, outer needle: 17G) (**Figure 2**A) was used for printing core/cladding fibers. A silicone tube extension was connected to the tip of the needle and an LED lamp was directed on the tube for in situ photocrosslinking of the Pluronic-DA,[19] and for triggering the onset of UV-PDMS crosslinking. Of the Pluronic-DA concentrations tested as cladding, the 33.3 wt.% system offered the best printability, since it has the lowest transition temperature (6.2–9.6 °C, Table S1, Supporting Information) and was therefore a fully-formed, shear-thinning physical gel at the printing temperature of 18 °C. The mechanical stability and handleability of the 33.3 wt.% claddings after crosslinking were also superior to the lower concentrations, and this composition was therefore used for all subsequent fibers. The photocrosslinked Pluronic-DA cladding acted as a supporting template for the PDMS core, whose crosslinking continued after extrusion. A second UV exposure step was used after printing to ensure full crosslinking of the UV-PDMS core over the next 24 h at room temperature since the radiant exposure delivered during in situ crosslinking was inferior to the recommended 2000 mJ cm^{-2} for full curing (data from manufacturer). In the case of T-PDMS, crosslinking of the liquid core was performed by heating the printed fiber at 37 °C for 48 h in a humid atmosphere.

By adjusting the printing conditions, smooth flexible fibers >50 cm in length with 1.0 mm outer diameter and 100–550 µm core diameters were printed in a continuous manner at speeds of 1–5 mm s^{-1} (Figure 2B), with the fiber length limited only by the capacity of the syringes. Optical microscopy of a representative printed fiber (Figure 2C) shows the distinct, smooth interface between core and cladding that is desirable for efficient waveguiding. The diameter of the core could be varied between 100 and 550 µm by adjusting the printing pressure of both core and cladding (for core: between 100 and 140 kPa; for cladding: between 300 and 360 kPa) and the power of the UV source between 30 and 70%. The core diameter increased with increasing pressure applied to the core solution, and decreased with increasing pressure applied to the cladding solution since

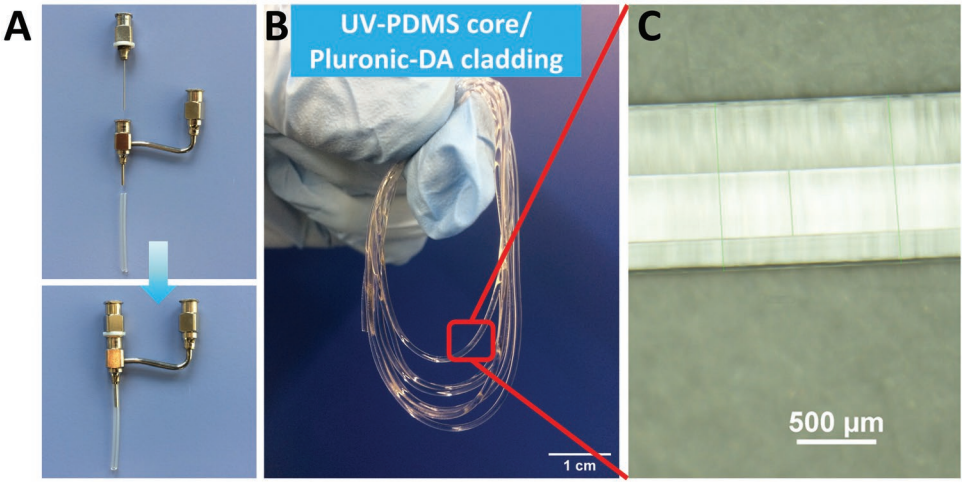

Figure 2. A) Image of the disassembled (top) and assembled (bottom) co-axial nozzle used to print the PDMS/Pluronic-DA core/cladding fibers, including the transparent silicone tube extension through which UV-photocrosslinking was performed. B) Macroscopic image of a printed flexible core/cladding optical waveguide. C) Microscopy image of the printed fiber showing the clear core/cladding structure.

a relatively higher pressure for the cladding corresponds to a higher cladding flow rate which forces the core to elongate and therefore decrease in diameter (Figures S4A,B, Supporting Information). No significant differences in these trends and values were observed between waveguides with T-PDMS or UV-PDMS cores. A higher UV irradiance increased the crosslinking rate of the Pluronic-DA cladding layer, resulting in greater contraction around the core PDMS which further decreased the core diameter (Figure S4C, Supporting Information).

2.4. Optical Performance of the Core/Cladding Optical Waveguides

Waveguiding performance was tested in a custom setup used for all optical loss measurements in this work (Scheme S2, Supporting Information). The auto-fluorescence intensity emitted perpendicular to the fiber axis was measured and assumed to be proportional to the propagating light intensity,[34] with a 550 nm long-pass wavelength filter between the fiber and the camera excluding scattered photons originating from the 405 nm light source. The optical loss $\alpha(\lambda)$ (in dB cm^{-1}) is defined as:

$$\alpha(\lambda) = (10/L)\log(I_0/I_L) \quad (1)$$

where I_0 is the intensity of side-emitted light at an arbitrary initial position, and I_L is the intensity at distance L (in cm) from the initial position. An optical loss value of 0.28 dB cm^{-1} was measured at 405 nm.

The optical loss of the waveguides in air was measured at different wavelengths (**Figure 3**A). The optical loss decreased with increasing wavelength for both waveguides due to lower scattering and absorption (Figure 1A), as visually observed in optical images of the fibers (Figure S5, Supporting Information). The optical loss values for the UV-PDMS fiber were lower than those of the T-PDMS fibers, with the difference most pronounced at 405 nm (0.3 vs 1.1 dB cm^{-1}). We attribute the lower optical loss of the UV-PDMS core/cladding waveguide to a more intimate core/cladding interface. In macroscopic tests, the core could be pulled out cleanly from the T-PDMS based fibers, while the removal of the core from UV-PDMS fibers resulted in fracture of the cladding (data not shown). A smoother, more cohesive core/cladding interface is important to minimize extrinsic waveguides losses.[35]

The optical loss values for the UV-PDMS waveguide were also measured in tissue. For this purpose, the waveguides were sandwiched between porcine muscle samples (Figure 3B). The obtained optical loss values (0.34 dB cm^{-1} at 405 nm, 0.13 dB cm^{-1} at 520 nm, Figure 3C) are comparable to those in air (Figure 3A), corroborating that light was confined to the UV-PDMS core and largely unaffected by the change in the external medium. T-PDMS showed markedly higher optical loss values in tissue than in air, with ≈threefold higher loss in tissue than in air at 520 nm. This is qualitatively evident in the optical images of the waveguides in Figure 3B. As in air, the optical loss values for T-PDMS in tissue were also significantly higher than for UV-PDMS. Optical loss values can be expressed as penetration depths to give a more intuitive representation of light delivery. Penetration depth (L_e) is defined as the distance at which the intensity of propagating light decreases to 1/e (≈37%) of its initial value. The penetration depths for the UV-PDMS waveguides in tissue range from 13 to 36 cm as wavelength increases from 405 to 520 nm (Figure 3D), which is in the target range for organ-scale light delivery in vivo. Longer wavelengths could not activate the auto-fluorescence necessary for optical loss quantification by the method used in this paper, but penetration depths of 670 and 808 nm light (depicted qualitatively in Figure 3B) are expected to be even greater than at 520 nm because absorbance decreases with increasing wavelength (Figure 1A). In contrast, the penetration depths for T-PDMS are significantly lower and range from 3.0 cm at 405 nm to 7.1 cm at 520 nm (Figure 3D). The UV-PDMS based waveguide therefore clearly outperforms its T-PDMS based counterpart for low-loss waveguiding in tissue.

The measured optical loss values of the printed UV-PDMS/Pluronic fibers are significantly lower than those of reported

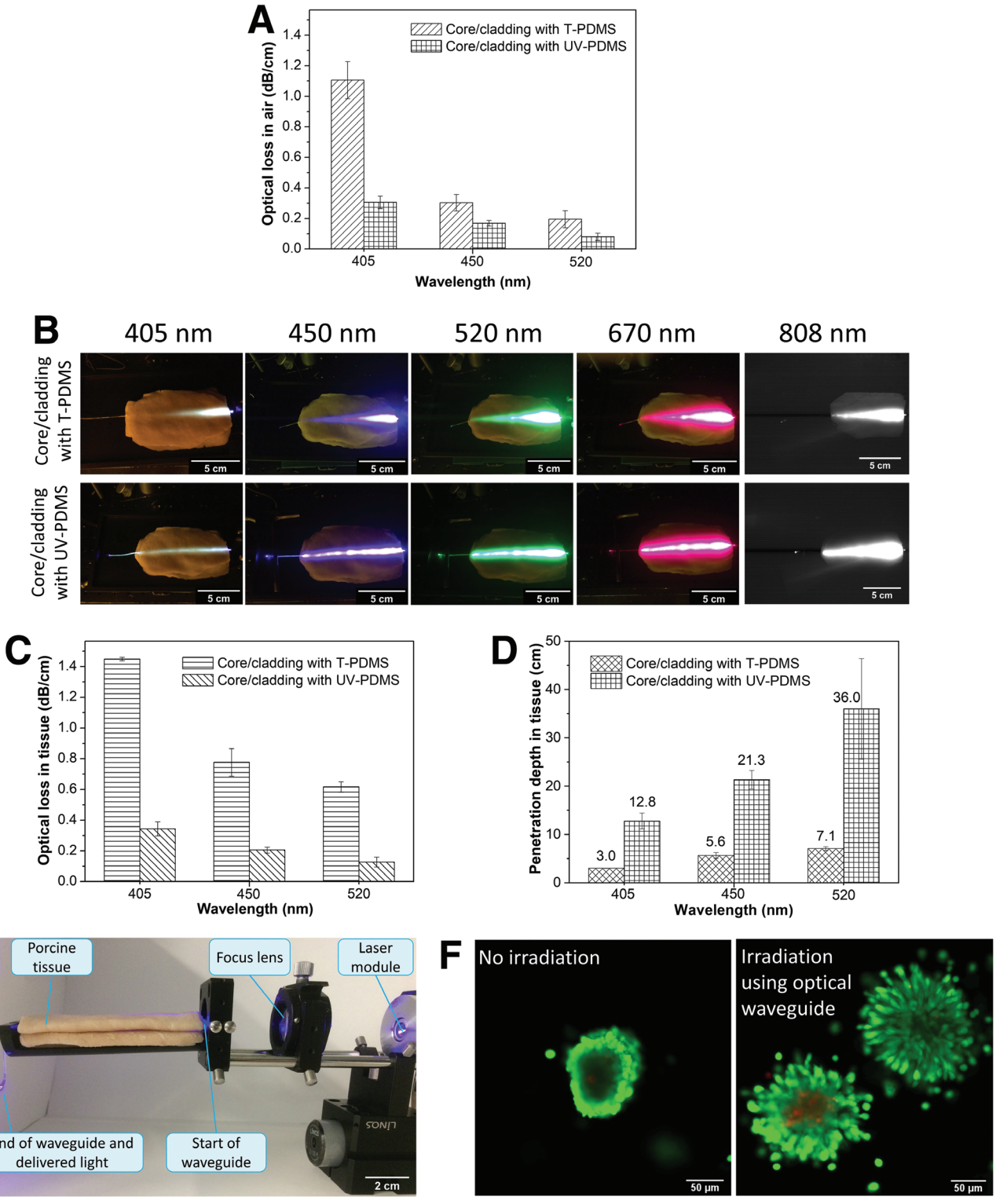

Figure 3. A) Optical loss of the T- and UV-PDMS/Pluronic-DA (33.3 wt.%) core/cladding waveguides in air. Data are presented as average ± standard deviation ($n = 3$). B) Optical images of T- and UV-PDMS/Pluronic core/cladding waveguides sandwiched between two pieces of 10 cm long tissue and in-coupled with different wavelengths of light. C) Optical loss and D) penetration depth of light guided by the UV-PDMS/Pluronic-DA (33.3 wt.%) core/cladding waveguide through tissue as shown in (B). Data are presented as average ± standard deviation ($n = 3$). E) Experimental design for delivering light to a 3D cell culture using printed waveguides passing through ex vivo tissue. F) Live/dead staining of fibroblast spheroids inside Dex-MA hydrogel modified with the photoactivatable cell adhesive peptide cyclo[RGD(DMNPB)fC] after two days of culture. The hydrogel was illuminated for 30 min at 405 nm using a UV-PDMS/Pluronic waveguide to activate the RGD units that support invasion of the gel by the fibroblasts (right image), while the control gel (left) was not illuminated and showed no cell migration.

PDMS-based fibers. For comparison, the all-PDMS core/cladding fibers reported by Guo et al. showed optical loss of 1.2 dB cm^{-1} at 500 nm,[6] and the single-material PDMS waveguides for scleral crosslinking showed optical loss of 0.5 dB cm^{-1} in contact with tissue at 445 nm.[13] The smooth core/cladding interface imparted by the printing process assisted by the Pluronic cladding, combined with the favorable RI difference between core and cladding, contribute to a better optical performance.

The possibility to activate photochemical reactions of relevance in photopharmacology and in the field of photoresponsive biomaterials for tissue regeneration was tested.[36] Fibroblast spheroids encapsulated in a dextran hydrogel modified with a photosensitive cell adhesive peptide[37] were irradiated with 405 nm light through a 12 cm printed waveguide sandwiched between 8 cm long tissue (Figure 3E). Light exposure was expected to activate the adhesive peptide (Figure S6, Supporting Information)[36a,b] and trigger cell attachment, proliferation, and migration. In-coupled light propagated through the tissue-surrounded waveguide to the distal end and illuminated the hydrogels. Exposed hydrogels after 2 days of cell culture showed migration of fibroblasts from the spheroids into the surrounding gel, while in non-exposed controls the fibroblasts remained confined in the spheroids (Figure 3F). These results demonstrate that the printed fibers can deliver light through tissue and activate photoresponsive biomaterials.

2.5. Stretchability and Optical Properties of the Printed UV-PDMS/Pluronic Waveguides

One of the key attractions of developing soft elastomeric waveguides is their extensibility, permitting light delivery in strained environments (i.e. heart, lung, or muscle).[10] The UV-PDMS and T-PDMS based core/cladding waveguides could be stretched to more than 5 times their original length without visible damage (**Figure 4**A,B; Figure S7A, Supporting Information), permitted by the elastomeric nature of both the PDMS and the Pluronic-DA. The combination of physical and covalent crosslinks in the Pluronic-DA cladding provided elasticity and toughness[22b] that were compatible with the mechanical properties of the PMDS core. No significant change in the optical loss was observed up to ≈200% strain (Figure 4C), indicating that the smooth core/cladding interface critical for effective light confinement was maintained.

Although the optical loss values were not significantly affected by strain over this range, strain inevitably reduces the cross-sectional area of the fiber and increases the length along which light needs to propagate in order to reach the distal end of a given fiber, meaning that the light intensity at the distal end decreased with increasing strain (Figure 4D,E; Figure S7B, Supporting Information). This expected result forms the principle of strain-sensing waveguides, which have been demonstrated in both hydrogel and elastomeric formats with dyes added to increase the sensitivity of strain sensing and allow independent strain measurements in different sections of a single fiber.[10,14] Although not the focus of this work, the flexible nature of these waveguides is also expected to facilitate waveguiding under bending, with increases in optical loss predictable from theory[38] and experimentally shown in literature to be typically <0.1 dB cm^{-1} at bending radii >1 cm and RI contrasts between core and cladding comparable to our fibers.[8,35]

3. Conclusion

Waveguides for biomedical applications are moving towards compliant and flexible materials fabricated by straightforward methods, with extrusion printing showing promise for this purpose. In the present work, an extrusion printing approach with a co-axial nozzle was used to produce waveguides with PDMS-based elastomeric cores and Pluronic-DA based hydrogel cladding. Both PDMS and Pluronic are clinically-approved polymers that have been extensively employed in various medical scenarios and are therefore appealing materials for biomedical waveguides. In situ photopolymerization of the shear-thinning Pluronic-DA cladding was a robust strategy for templating the slower-crosslinking PDMS liquid cores, allowing the fabrication of core/cladding fibers in a single step. The mechanical and optical properties of crosslinked Pluronic-DA are complementary to those of crosslinked PDMS used for the waveguide core, generating stretchable optical fibers. Of the two types of PDMS tested, the UV-cured variant was the standout performer, with UV-PDMS/Pluronic-DA core/cladding waveguides showing optical loss values of 0.34 dB cm^{-1} at 405 nm and 0.13 dB cm^{-1} at 520 nm in tissue. These values are essentially unchanged from those obtained in air, indicating excellent light confinement in the core, and are lower than reported values for other PDMS-based biomedical waveguides measured at comparable wavelengths. The developed fibers can therefore be envisaged for therapeutic and sensing scenarios in vivo that require deep light delivery at locations in soft tissue that demand high compliance and extensibility, like a muscle or the heart. From a fabrication perspective, the present work opens up new possibilities for the fabrication of optical devices from medically-approved polymers. As extrusion printing technologies continue to evolve, the waveguides in this work may be integrated with other printed optical and therapeutic materials to give multifunctional therapeutic devices through a single streamlined fabrication approach.

4. Experimental Section

Synthesis of Pluronic-DA: Pluronic-DA was synthesized following a reported protocol (Scheme S1, Supporting Information).[30] Pluronic F127 (20 g, 1.59 mmol, 1 equiv, Sigma Aldrich) and triethylamine (0.55 mL, 3.95 mmol, 2.5 equiv, Sigma Aldrich) were dissolved in dry dichloromethane (200 mL, Sigma Aldrich) in a 500 mL round-bottom flask. Then acryloyl chloride (0.26 mL, 3.08 mmol, 2 equiv, Sigma Aldrich) was added dropwise. The mixture was stirred on the ice for 12 h and then at room temperature for 12 h. After the reaction, the mixture was filtered and the volume reduced to ≈30 mL by rotary evaporation (37 °C, 200 mbar, BÜCHI Labortechnik AG). The crude product was purified by precipitation into 500 mL of diethylether and dried under vacuum for 2 days. The extent of acrylate functionalization was determined by ^{1}H NMR spectroscopy (Figure S1A,B, Supporting Information). The new peaks at 5.98–6.52 ppm confirmed the attachment of acryloyl groups. The extent of acrylation was determined by comparing the integral of these acrylic

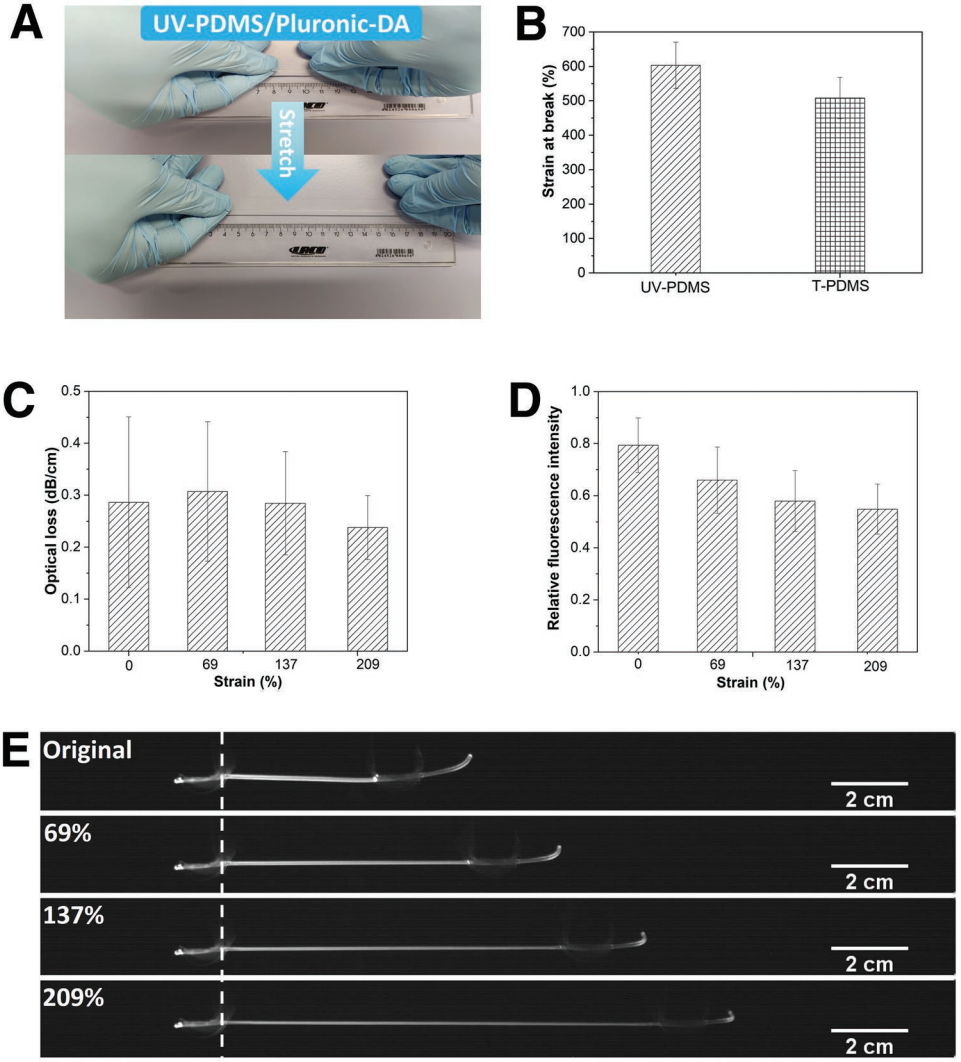

Figure 4. A) Stretching of printed UV-PDMS/Pluronic-DA (33.3 wt.%) core/cladding optical fibers. B) The strain at break of printed core/cladding fibers measured by tensile testing. Data are presented as average ± standard deviation ($n = 5$). C) The optical loss in UV-PDMS based core/cladding fibers under different strains. Data are presented as average ± standard deviation ($n = 6$). D) Auto-fluorescence intensity at the distal end of UV-PDMS based core/cladding fibers relative to the auto-fluorescence intensity at the proximal end. Data are presented as average ± standard deviation ($n = 6$). E) The images of auto-fluorescence of fibers under different strains used to construct (C) and (D), with the dotted line indicating the point at which the fiber emerges from the clamp at the proximal end. The point at which the fiber enters the clamp at the distal end is clearly observed at the end of the straight section. In-coupled wavelength: 405 nm. Detection wavelength: > 550 nm.

protons to the integral of the methyl groups (1.05–1.28 ppm) from the propylene oxide units in the polymer backbone. The measured degree of substitution was 70%.

Physiochemical Characterization of Pluronic-DA Hydrogels: The characterization of the sol-gel transition temperature of Pluronic-DA solutions at different concentrations (16.7–33.3 wt.%) was performed by rheology (DHR 3 rheometer, TA Instruments) in a temperature-sweep experiment, in oscillation mode, using a parallel plate geometry with 20 mm stainless steel plates and the gap was set as 200 µm. The temperature was increased from 5 °C to 37 °C at a rate of 5 °C min^{-1}. Measurements were performed at 0.5% strain and 1 Hz frequency. The shear thinning behavior of Pluronic-DA hydrogels at room temperature was characterized in a rotation mode, within the range of shear rates from 0.01 s^{-1} to 1000 s^{-1}. For this experiment, the Pluronic-DA solutions were loaded between the two parallel plates and kept at room temperature for 10 min to allow the hydrogel to form, after which the flow sweep measurement was started.

The shear elastic moduli of physically and covalently crosslinked Pluronic-DA hydrogels at different concentrations (23.1–33.3 wt.%) were measured by rheometry in time sweep experiments at room temperature using the parallel plate geometry with 20 mm stainless steel plates, and a gap 200 µm. Irgacure 2959 was added as initiator at 0.2 wt.%. A 0.5% strain and 1 Hz frequency were used for the measurements. The first 5 min of the experiments were performed without light exposure, followed by a further 5 min during which the hydrogel was illuminated at 365 nm (10 mW cm^2) to trigger photoinitiated crosslinking. The Young's Modulus (E) was calculated from the storage modulus (G') and Poisson ratio (for hydrogels, $\nu = 0.45$–0.5, in the present work 0.5 was adopted) using Equation 2:[39]

$$E = 2G(1+\nu) \quad (2)$$

The swelling ratio of Pluronic-DA hydrogels with different polymer concentrations was calculated by Equation 3:

$$SR = \frac{W_s - W_d}{W_d} \times 100\% \quad (3)$$

where SR is the swelling ratio, W_s is the weight of the swollen hydrogel, and W_d is the weight of the dry polymer. The samples were obtained by photopolymerization of Pluronic-DA solutions containing Irgacure 2959 (0.3 wt.%) as initiator in a Teflon mold with a 5 mm diameter. The hydrogels were then immersed in water for 24 h and weighed to obtain the swollen mass. Then the hydrogels were freeze-dried and the dry mass was determined.

Characterization of Optical Properties of Pluronic-DA Hydrogels: The transparency of Pluronic-DA hydrogels was characterized by measuring the light absorbance in the spectral range from 350 to 800 nm. The samples were prepared in standard 1 cm wide poly(methyl methacrylate) disposable cuvettes by photopolymerization. The hydrogel precursor contained a given concentration of Pluronic-DA and 0.3 wt.% of Irgacure 2959 as initiator. The precursors were pipetted into the cuvettes and irradiated at 365 nm (1 mW cm^{-2}) using a UV lamp (LTF-Labortechnik) for 15 min. Light absorbance was measured with a conventional UV–vis spectrophotometer (Cary 4000, Agilent Technologies).

The scattering of the Pluronic-DA hydrogels was measured using a custom setup as shown in Scheme S3 (Supporting Information). Hydrogel samples were prepared in the same way as for absorbance measurements. A 520 nm laser (CrystaLaser) was focused and directed perpendicular to the hydrogel. A camera (Thorlabs) was placed at 90° to the laser path and images of the scattered light were taken. The laser power (500 mW) and exposure time (5 ms) of the camera were fixed. The intensity of the scattered light from the images was quantified using the free software ImageJ. The average scattering intensity of Pluronic-DA 23.1 wt.% hydrogel was set as the reference and used to normalize the scattering intensity of the other hydrogels.

The refractive indices of Pluronic-DA hydrogels were measured with a refractometer (Anton Paar) at 20 °C and at 589.3 nm. Hydrogel samples were prepared in a Teflon mold with a diameter of 5 mm and a depth of 2 mm. The hydrogel precursors contained Pluronic-DA at defined concentrations and 0.3 wt.% of Irgacure 2959 as initiator. 40 µL of precursor solution was injected in the mold and covered by a coverslip. The samples were illuminated at 365 nm (1 mW cm^{-2}) for 15 min in order to photoinitiate crosslinking of the DA functions.

Printing of Optical Waveguides: A 3D-Bioscaffolder (GeSiM, Dresden) was used for printing.[19] The cooled 33.3 wt.% Pluronic-DA inks including 0.3 wt.% Irgacure 2959 as initiator were loaded into UV-blocked syringes (Fluid dispensing system, Nordson) and kept on ice until all bubbles disappeared, and then kept at room temperature to allow the formation of physically crosslinked hydrogels. After that, the syringe was mounted onto the printhead and connected to the pneumatic tube. The printing coaxial needle (Coaxial Spinneret Needle, inner needle: 22G, outer needle: 17G, Leonardino) was extended with a transparent silicone tube (1.02 mm inner diameter, Mono-Lumen Tubing, Freudenberg Medical) to allow photopolymerization of the printed thread. The UV lamp (Series 1500, OmniCure) was adjusted to focus on the silicone tube with a defined UV intensity (from 30 to 70%).

For printing the core/cladding structure, thermocurable polydimethylsiloxane (T-PDMS: Dow Corning, Sylgard 184 Silicone Elastomer) and UV-curable PDMS (UV-PDMS: Shin-Etsu, KER-4690) were used as core, and 33.3 wt.% Pluronic-DA was used as cladding. For the preparation of the T-PDMS precursor, the prepolymer and crosslinking agent were mixed in a weight ratio of 10:1. For UV-PDMS, the two components were mixed at a weight ratio of 1:1. The bubbles in the prepared mixtures were removed under vacuum for 30 min. The mixture was loaded into the UV-blocked syringe and connected to the pneumatic tube. Core/cladding filaments were produced by providing pressure to both channels. The order of switching on and off the pressure of the channels, to initialize the printing, was very important for successful printing of the core/cladding structures. The pressure of the core was applied first, followed by applying the pressure on the cladding. To stop printing, the pressure to the core was stopped after stopping pressure on the cladding. After printing, the core/cladding waveguides with T-PDMS were irradiated by 365 nm UV light (1 mW cm^{-2}) for 20 min to get a fully crosslinked cladding layer, and then stored in a sealed box (with wet tissue paper to keep the humidity) and kept in the oven at 37 °C for 48 h. The waveguides with UV-PDMS were further irradiated by 365 nm UV light (1 mW cm^{-2}) for 20 min and stored in a humid environment for 24 h at room temperature to get a fully crosslinked core. The post-treated waveguides were stored in a sealed box with wet tissue paper to keep the humidity.

The effect of pressure and UV intensity on the diameter of the waveguide core was studied. The 2.5 cm length of the silicone tube, 0.3 wt.% initiator concentration, and 33.3 wt.% of Pluronic-DA were fixed in all the experiments. For the study of the effect of pressure, the UV intensity was set at 60%. For the study of the effect of UV intensity, the pressure for the core and cladding were set at 120 and 340 kPa respectively.

Characterization of Light Guiding Properties of Printed Waveguides: The optical loss was measured with a custom setup by adapting optical loss measurement protocols from previous reports[34] (shown in Scheme S2, Supporting Information). A laser (Compact Laser Modules with Phono Jack, 405/450/520 nm wavelengths, 4.5 mW, Thorlabs) was focused on the proximal end of each printed fiber through a planoconvex lens (f80, quartz glass, LINOS). The autofluorescence of the material was activated when light propagated in the fiber. The autofluorescence was captured by a camera with a long-pass filter (550 nm) which was set perpendicular to the fiber axis. With the captured picture, the intensity of auto-fluorescence along the fiber was analyzed using ImageJ. The attenuation coefficient (optical loss) was calculated according to Equation 1 (see Section 2.4, main paper).

For measuring the optical loss in tissue, the fiber was sandwiched between two pieces of porcine muscle tissue. The intensity of the auto-fluorescence of the fiber immediately before entering and immediately after exiting the tissue was used to calculate the optical loss.

For measuring the optical loss under stretching, the fibers were clamped with two clamps. One clamp was kept in one position to allow stable light in-coupling as described above. Strain was calculated by the following equation:

$$\text{Strain} = (L - L_0)/L_0 \times 100\% \quad (4)$$

where L_0 is the initial distance between the two clamps, and L is the actual distance between two clamps. The optical loss was measured at different strains by moving the distal end to different distances.

Measurement of Stretchability: The stretchability of fibers was measured by tensile test (ElectroForce 3200, TA Instruments). The fiber was fixed by two clamps with an initial distance of 1.5 cm. The moving speed of the motor was set at 1 mm s^{-1}. The maximum strain, calculated based on the distance between the clamps similarly to the previous section, was obtained when the fiber was broken.

Application of Printed Optical Fibers in Controlling Cell Migration

Cell-Adhesive Peptide: Cyclic RGDfC peptide was synthesized by solid-phase peptide synthesis (SPPS) according to a previous report.[40]

Cell Culture: Fibroblast L929 cell line was cultivated at 37 °C in 5% CO_2 in RPMI medium (Gibco) supplemented with 10% fetal bovine serum (Invitrogen) and 1% P/S (Invitrogen). Cells were used between passages P4 and P16.

Gel Formation with Spheroids: Twenty thousand cells were seeded in each well of a Corning Costar Ultra-Low attachment multiwell plate and incubated for 48 h. The cell medium was then removed carefully and the spheroids were washed once with PBS. Spheroids were collected into Eppendorf tubes and spun down for 30 s at 300 rpm. PBS was carefully removed.

Dextran-methacrylate (MA) was synthesized by following a previous protocol.[41] DexMA solution was prepared by dissolving DexMA (20 mg) in TEOA buffer (100 µL, pH 9.5) under sterile laminar flow. Cyclo[RGD(DMNPB)fC] (4.2 mg mL^{-1}, 5 mM) were freshly prepared in sterilized water from Cellendes (pH 5). Constant concentrations were used during all experiments. DexMA solution (20 µL) and cyclo[RGD(DMNPB)fC] solution (5 µL) were mixed and incubated for

30 min at 37 °C. TEOA buffer containing spheroids (10 µL) was added into the solution followed by adding CD link (5 µL, 20 mmol L^{-1} thiol groups). 10 µL of the solution was put into each well of Ibidi 15 µwell angiogenesis slide. The slide was put upside down for 15 min in the incubator for gelation. After gelation, the slide was inverted, and 50 µL of cell medium was added on top of the hydrogels.

Photoactivation of Hydrogel Using Optical Fibers Passing Through Tissue: As shown in Figure 3E, a printed fiber (length: 12 cm) was sandwiched between two pieces of pig muscle tissue (8 cm in length, 2 mm in thickness). A laser (405 nm, 5 mW, ThorLabs) was focused on one end of the fiber. The light was delivered to the top of DexMA hydrogel containing cell spheroids by propagating in the fiber through the tissue for 30 min. The cell medium was changed once after light exposure, and the culture was incubated under the protection from light.

Live/Dead Assay: After two days, a live/dead assay was performed to visualize the cell viability and spheroid morphology. The cell culture medium was removed and samples were incubated for 5 min with fluorescein diacetate (40 µg mL^{-1}, Sigma, F7378) and propidium iodide (30 µg mL^{-1}, Sigma, P4170) in PBS. Samples were washed twice with PBS and imaged with Zeiss LSM 800 confocal microscope.

Statistical Analysis: Statistical analysis data for each graph is specified in the figure caption.

Supporting Information

Supporting Information is available from the Wiley Online Library or from the author.

Acknowledgements

S.P. and A.D.C. received funding from the European Union's Horizon 2020 research and innovation program under the FET PROACTIVE grant agreement no. 731957 (Mechano-Control). J.F. and Q.J. acknowledge financial support from the China Scholarship Council (CSC).

Open access funding enabled and organized by Projekt DEAL.

Conflict of Interest

The authors declare no conflict of interest.

Data Availability Statement

The data that support the findings of this study are available from the corresponding author upon reasonable request.

Keywords

elastomers, extrusion printing, hydrogels, optical fibers, optical waveguides, photoactivations

Received: November 19, 2021
Revised: March 22, 2022
Published online: April 26, 2022

[1] S. Shabahang, S. Kim, S.-H. Yun, *Adv. Funct. Mater.* **2018**, *28*, 1706635.

[2] a) A. N. Zorzos, E. S. Boyden, C. G. Fonstad, *Opt. Lett.* **2010**, *35*, 4133; b) B. Rubehn, S. B. E. Wolff, P. Tovote, A. Luethi, T. Stieglitz, *Lab Chip* **2013**, *13*, 579.

[3] A. Canales, S. Park, A. Kilias, P. Anikeeva, *Acc. Chem. Res.* **2018**, *51*, 829.

[4] a) C. Lu, U. P. Froriep, R. A. Koppes, A. Canales, V. Caggiano, J. Selvidge, E. Bizzi, P. Anikeeva, *Adv. Funct. Mater.* **2014**, *24*, 6594; b) A. Canales, X. Jia, U. P. Froriep, R. A. Koppes, C. M. Tringides, J. Selvidge, C. Lu, C. Hou, L. Wei, Y. Fink, P. Anikeeva, *Nat. Biotechnol.* **2015**, *33*, 277; c) C. Lu, S. Park, T. J. Richner, A. Derry, I. Brown, C. Hou, S. Rao, J. Kang, C. T. Moritz, Y. Fink, P. Anikeeva, *Sci. Adv.* **2017**, *3*, e1600955; d) S. Park, Y. Guo, X. Jia, H. K. Choe, B. Grena, J. Kang, J. Park, C. Lu, A. Canales, R. Chen, *Nat. Neurosci.* **2017**, *20*, 612.

[5] a) J. Guo, C. Yang, Q. Dai, L. Kong, *Sensors* **2019**, *19*, 3771; b) M. Umar, K. Min, S. Kim, *APL Photonics* **2019**, *4*, 120901.

[6] J. Guo, B. Zhou, C. Yang, Q. Dai, L. Kong, *Adv. Funct. Mater.* **2019**, 1902898.

[7] F. Abbasi, H. Mirzadeh, A.-A. Katbab, *Polym. Int.* **2001**, *50*, 1279.

[8] J. Missinne, S. Kalathimekkad, B. Van Hoe, E. Bosman, J. Vanfleteren, G. Van Steenberge, *Opt. Express* **2014**, *22*, 4168.

[9] a) J. Missinne, G. Van Steenberge, B. Van Hoe, K. Van Coillie, T. Van Gijseghem, P. Dubruel, J. Vanfleteren, P. Van Daele, presented at *Photonics Packaging, Integration, and Interconnects IX*, **2009**; b) C. K. Harnett, H. Zhao, R. F. Shepherd, *Adv. Mater. Technol.* **2017**, *2*, 1700087; c) A. Ersen, M. Sahin, *J. Biomed. Opt.* **2017**, *22*, 055005.

[10] J. Guo, X. Liu, N. Jiang, A. K. Yetisen, H. Yuk, C. Yang, A. Khademhosseini, X. Zhao, S. H. Yun, *Adv. Mater.* **2016**, *28*, 10244.

[11] a) L. Wang, C. Zhong, D. Ke, F. Ye, J. Tu, L. Wang, Y. Lu, *Adv. Opt. Mater.* **2018**, *6*, 1800427; b) Y. Zhang, A. D. Mickle, P. Gutruf, L. A. McIlvried, H. Guo, Y. Wu, J. P. Golden, Y. Xue, J. G. Grajales-Reyes, X. Wang, S. Krishnan, Y. Xie, D. Peng, C.-J. Su, F. Zhang, J. T. Reeder, S. K. Vogt, Y. Huang, J. A. Rogers, R. W. Gereau, *Sci. Adv.* **2019**, *5*, eaaw5296.

[12] H. Zhao, K. O'Brien, S. Li, R. F. Shepherd, *Sci. Rob.* **2016**, *1*, eaai7529.

[13] S. J. Kwok, M. Kim, H. H. Lin, T. G. Seiler, E. Beck, P. Shao, I. E. Kochevar, T. Seiler, S.-H. Yun, *Investi. ophthalmol. visual sci.* **2017**, *58*, 2596.

[14] J. Guo, M. Niu, C. Yang, *Optica* **2017**, *4*, 1285.

[15] M. Ramuz, B. C. K. Tee, J. B. H. Tok, Z. Bao, *Adv. Mater.* **2012**, *24*, 3223.

[16] C. To, T. L. Hellebrekers, Y.-L. Park, presented at *2015 IEEE/RSJ International Conference on Intelligent Robots and Systems (IROS)*, **2015**.

[17] Z. Cai, W. Qiu, G. Shao, W. Wang, *Sens. Actuators, A* **2013**, *204*, 44.

[18] I. Martincek, D. Pudis, M. Chalupova, *IEEE Photonics Technol. Lett.* **2014**, *26*, 1446.

[19] L. Ouyang, C. B. Highley, W. Sun, J. A. Burdick, *Adv. Mater.* **2017**, *29*, 1604983.

[20] a) G. Dumortier, J. L. Grossiord, F. Agnely, J. C. Chaumeil, *Pharm. Res.* **2006**, *23*, 2709; b) J. Suksiriworapong, T. Rungvimolsin, A. Atitaya, V. B. Junyaprasert, D. Chantasart, *AAPS PharmSciTech* **2014**, *15*, 52.

[21] G. Dumortier, J. Grossiord, M. Zuber, G. Couarraze, J. Chaumeil, *Drug Dev. Ind. Pharm.* **1991**, *17*, 1255.

[22] a) V. Lenaerts, C. Triqueneaux, M. Quartern, F. Rieg-Falson, P. Couvreur, *Int. J. Pharm.* **1987**, *39*, 121; b) J. J. Escobar-Chávez, M. López-Cervantes, A. Naik, Y. Kalia, D. Quintanar-Guerrero, A. Ganem-Quintanar, *J. Pharm. Pharm. Sci.* **2006**, *9*, 339.

[23] X. Liu, H. Yuk, S. Lin, G. A. Parada, T. C. Tang, E. Tham, C. de la Fuente-Nunez, T. K. Lu, X. Zhao, *Adv. Mater.* **2018**, *30*, 1704821.

[24] D. J. Lorang, D. Tanaka, C. M. Spadaccini, K. A. Rose, N. J. Cherepy, J. A. Lewis, *Adv. Mater.* **2011**, *23*, 5055.

[25] J. Feng, Y. Zheng, S. Bhusari, M. Villiou, S. Pearson, A. del Campo, *Adv. Funct. Mater.* **2020**, *30*, 2004327.

[26] a) Y.-n. Sun, G.-r. Gao, G.-l. Du, Y.-j. Cheng, J. Fu, *ACS Macro Lett.* **2014**, *3*, 496; b) C.-J. Wu, A. K. Gaharwar, B. K. Chan, G. Schmidt, *Macromolecules* **2011**, *44*, 8215.
[27] S. Joas, G. E. M. Tovar, O. Celik, C. Bonten, A. Southan, *Gels* **2018**, *4*, 69.
[28] a) L. H. de Oliveira, R. R. Pinto, E. d. S. Monteiro Filho, M. Aznar, *J. Chem. Eng. Data* **2021**, *66*, 2959; b) O. V. Elisseeva, N. A. M. Besseling, L. K. Koopal, M. A. Cohen Stuart, *Langmuir* **2005**, *21*, 4954.
[29] S.-Y. Lee, G. Tae, *J. Controlled Release* **2007**, *119*, 313.
[30] M. R. Kim, T. G. Park, *J. Controlled Release* **2002**, *80*, 69.
[31] W. E. Hennink, C. F. van Nostrum, *Adv. Drug Delivery Rev.* **2012**, *64*, 223.
[32] a) Z. Brounstein, J. Zhao, D. Geller, N. Gupta, A. Labouriau, *Polymers* **2021**, *13*, 3125; b) R. Y. Lukin, A. M. Kuchkaev, A. V. Sukhov, G. E. Bekmukhamedov, D. G. Yakhvarov, *Polymers* **2020**, *12*, 2174.
[33] E. C. Murphy, J. H. Dumont, C. H. Park, G. Kestell, K.-S. Lee, A. Labouriau, *J. Appl. Polym. Sci.* **2020**, *137*, 48530.
[34] a) D. Di Camillo, V. Fasano, F. Ruggieri, S. Santucci, L. Lozzi, A. Camposeo, D. Pisignano, *Nanoscale* **2013**, *5*, 11637; b) F. Gu, H. Yu, P. Wang, Z. Yang, L. Tong, *ACS Nano* **2010**, *4*, 5332; c) D. O'Carroll, I. Lieberwirth, G. Redmond, *Small* **2007**, *3*, 1178.
[35] M. Choi, M. Humar, S. Kim, S.-H. Yun, *Adv. Mater.* **2015**, *27*, 4081;
[36] a) Y. Zheng, M. K. L. Han, Q. Jiang, B. Li, J. Feng, A. del Campo, *Mater. Horiz.* **2019**; b) A. Farrukh, J. I. Paez, A. del Campo, *Adv. Funct. Mater.* **2019**, *29*, 1807734; c) S. Petersen, J. M. Alonso, A. Specht, P. Duodu, M. Goeldner, A. del Campo, *Angew. Chem., Int. Ed.* **2008**, *47*, 3192; d) M. Wirkner, S. Weis, V. San Miguel, M. Álvarez, R. A. Gropeanu, M. Salierno, A. Sartoris, R. E. Unger, C. J. Kirkpatrick, A. del Campo, *ChemBioChem* **2011**, *12*, 2623; e) M. J. Salierno, A. J. García, A. del Campo, *Adv. Funct. Mater.* **2013**, *23*, 5974.
[37] Y. Zheng, M. K. L. Han, Q. Jiang, B. Li, J. Feng, A. del Campo, *Mater. Horiz.* **2020**, *7*, 111.
[38] R. T. Schermer, J. H. Cole, *IEEE J. Quantum Electron.* **2007**, *43*, 899.
[39] S. R. Caliari, J. A. Burdick, *Nat. Methods* **2016**, *13*, 405.
[40] T. T. Lee, J. R. García, J. I. Paez, A. Singh, E. A. Phelps, S. Weis, Z. Shafiq, A. Shekaran, A. Del Campo, A. J. García, *Nat. Mater.* **2015**, *14*, 352.
[41] B. M. Baker, B. Trappmann, W. Y. Wang, M. S. Sakar, I. L. Kim, V. B. Shenoy, J. A. Burdick, C. S. Chen, *Nat. Mater.* **2015**, *14*, 1262.